# Torque Ripple Analysis of a PM Brushless DC Motor Using Finite Element Method

Min Dai, *Student Member, IEEE*, Ali Keyhani, *Fellow, IEEE*, and Tomy Sebastian, *Senior Member, IEEE*

***Abstract*—Three-phase permanent magnet brushless dc motors are widely used. As a function of the rotor position, the torque produced by these machines has a pulsating component in addition to the dc component. This pulsating torque has a fundamental frequency corresponding to six pulses per electrical revolution of the motor. The shape of the torque waveform and, thus, the frequency content of the waveform can be influenced by several factors in the motor design and construction. This paper addresses the various factors that influence the torque waveshape. It is shown that in addition to the basic induced electromotive force (EMF) waveshape, the magnetic saturation in the stator core, and the accuracy in the skewing are also key factors in determining the torque waveshape. Computer simulation using finite element technique has been conducted to study the torque waveform. Simulation results successfully duplicated the torque waveforms measured in experiments under different excitation currents.**

***Index Terms*—Brushless machines, cogging, design methodology, finite element methods, permanent magnet machines, permanent magnet motors, torque ripple.**

## I. Introduction

TORQUE ripple is a critical concern in many applications where low acoustic noise, high efficiency, or friendly human-machine interactions are highly demanded. In the automotive industry, electrical power steering systems are being developed to replace the traditional hydraulic systems, where an electric motor is used as the actuator. In such a system, the motor shaft is connected to the steering wheel through a gearbox. Therefore, the motor torque pulsation must be small enough so that the driver would not be able to feel it.

Permanent magnet (PM) brushless dc motors have been widely used for their ease of control. However, a drawback of this type of machine, which limits their applications, is the characteristic torque ripple caused by the commutation of current from one phase to another, nontrapezoidal back-emf, and cogging. Therefore, as a candidate for electrical power steering actuator, this type of motors cannot be practically applied until the torque ripple problem is solved. Much research has been performed to analyze and reduce the torque ripple of PM brushless dc motors. Some have considered the torque ripple problem mainly from a design aspect, such as [1]–[14], while others have emphasized drive and control aspects, such as [15]–[17]. However, a phenomenon observed from experimental test data of a PM brushless dc motor, which is believed design related, has not been addressed by existing research. Experimental measurement of the torque of the motor [7] at low speed showed unexpected dips on the ripple of the torque waveform as a function of rotor position. This phenomenon is illustrated conceptually in Fig. 1, where the solid curve refers to the measured torque ripple. The position and shape of the dips vary with excitation current. The cause of such unexpected behavior is a serious concern for machine designers, especially in applications where torque ripple is critical. Recognition of the formation mechanism of the dips is undoubtedly the first step in determining whether anything, such as to control the magnitude or the position of the dip by changing design parameters either in geometry or materials, can be done in the machine design to reduce net torque ripple.

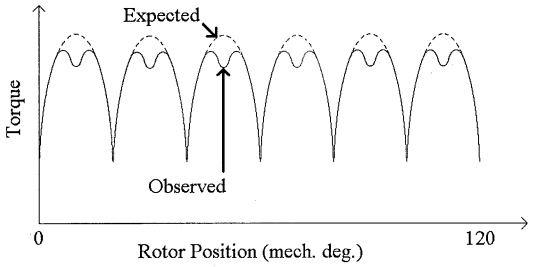


Fig. 1. Expected and observed torque ripple shapes.

Finite element analysis (FEA) is a powerful and economical approach to characterize the torque ripple of a given design without hardware prototyping, and makes it easy to change parameters to run different design scenarios. Therefore, it has been used in previous research concerning torque ripple of PM brushless dc machines as presented in [3], [7], [12], [18], and [19]. In this research, two-dimensional (2-D) FEA has been conducted to compute the torque waveform of the motor that was studied in [7]. The goal of the simulation is to compare the computed torque waveforms with the actual torque waveforms measured under various excitation currents and analyze the causes of the dip on the torque ripple.

In this paper, the machine model will be introduced, the method of analysis will be presented, the FEA-based simulation results will be validated using experimental data and Fourier analysis, and the effects of excitation current and skew angle will be discussed based on analysis of the FEA results.

## II. Model of the Machine

The PM brushless dc motor analyzed in this paper is a three-phase, six-pole, 18-slot machine. For torque ripple

Manuscript received November 27, 2000; revised March 19, 2002. This work was supported in part by Delphi Automotive Systems and in part by Magsoft Corporation.

M. Dai and A. Keyhani are with the Department of Electrical Engineering, The Ohio State University, Columbus, OH 43210 USA (e-mail: daim@ee.eng.ohio-state.edu; keyhani@ee.eng.ohio-state.edu).

T. Sebastian is with Delphi Saginaw Steering Systems, Saginaw, MI 48601 USA (e-mail: tomy.sebastian@delphiauto.com).

Digital Object Identifier 10.1109/TEC.2003.819105

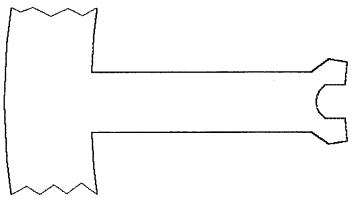

Fig. 2. Bifurcated tooth stator structure.

reduction considerations, a bifurcated tooth structure is used on the stator teeth as shown in Fig. 2.

Bifurcation reduces the variation in reluctance as seen by the magnet and consequently reduces the cogging torque and doubles the frequency of cogging [7]. The bifurcated tooth structure has been optimized to obtain the maximum reduction in cogging torque. The dummy slot formed by the bifurcation acts as a true slot from the view of rotor magnets. Therefore, a half stator slot skew can be used to minimize the cogging torque and meanwhile avoid making the line-to-line induced voltage waveform more sinusoidal than trapezoidal [7]. For manufacturing convenience, the stator slots are straight slots and the skewing effect is implemented by skewing the rotor magnets or rotor magnetization pattern. The rotor of the motor has six nonsalient, high energy Nd–Fe–B magnet poles that are magnetized in the radial direction.

## III. Method of Analysis

### A. FEA and the Software Used

2-D time stepping finite element analysis has been performed to compute the magnetic field and the torque generated by the motor at different rotor positions under different excitation currents. The FEA software tool Magsoft Flux2d® was used in this simulation. The preprocessing, calculation, and postprocessing were performed following [20]. The fundamental theory of finite element method behind the software can be found in [21]. The equiflux lines on a 60° cross-section model at a certain rotor position are shown in Fig. 3.

### B. Issues in the Simulation

A three-phase brushless dc motor fed by an inverter (as shown in Fig. 4) has six switching patterns $S1+S2$, $S2+S3$, $S3+S4$, $S4+S5$, $S5+S6$, and $S6+S1$, sequentially. Each of the switching patterns lasts for a period of 60 electrical degrees (20 mechanical degrees for a six-pole machine). During each switching period, two of the three phases are conducting. In steady state, the electromagnetic torque generated in the air-gap repeats itself in different switching periods. Therefore, it is enough to study the torque within only one switching period.

Under a stationary stator magnetomotive force (MMF) generated by any certain switching pattern, motoring electromagnetic torque is generated while the center axis of the rotor MMF rotates from the position of 180 electrical degrees apart from the center axis of the stator MMF to the position aligned with the center axis of the stator MMF. The torque waveform over this 180° (electrical) region is approximately trapezoidal plus cogging as shown in Fig. 5.

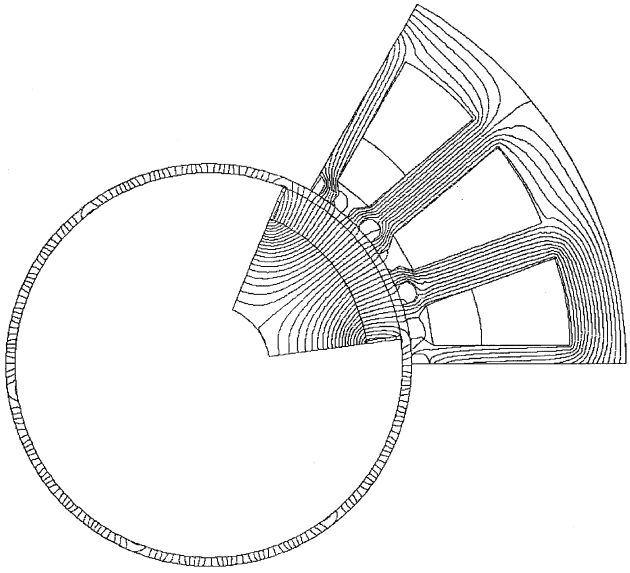

Fig. 3. Equiflux lines under 25-A current on a 60° cross section model when the rotor has rotated for 7.5° from its starting position.

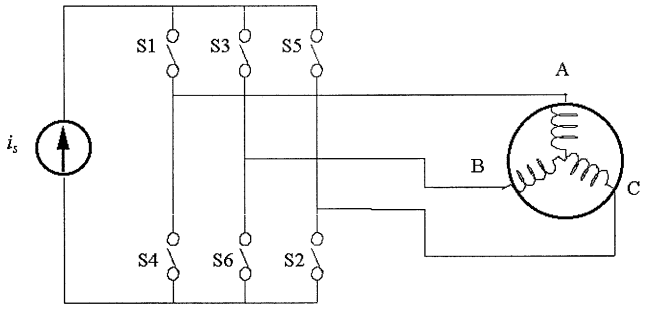


Fig. 4. Drive system for a three-phase brushless dc motor.

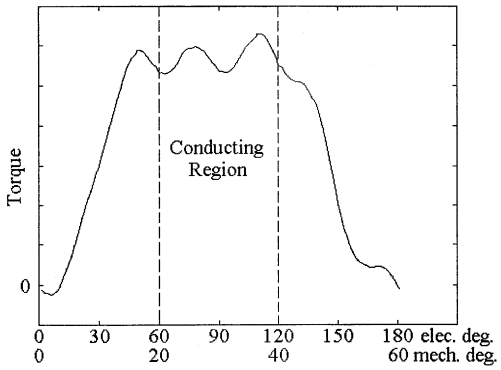


Fig. 5. Torque waveform over 180° (elec.) under a fixed switching pattern.

In practical applications, only 60° (elec.) out of the 180° is conducting due to the commutation. In order to maximize the output torque, the 60° region is centered at 90°. The conducting region is selected to be from 60° to 120° (the area between the dashed lines in Fig. 5). Therefore, the FEA study of the motor only needs to cover this 60° (elec.) region. Since the PM motor studied has a rotor magnet skew angle of a half slot pitch (10 mechanical degrees), skew effect must be considered when calculating the torque. However, 2-D FEA does not output torque waveforms with skew effects directly.

### C. Simulating the Skew Effects

An equivalent result of torque waveform with skewing effects can be obtained by averaging the 2-D FEA results over the skew angle based on the trapezoidal integration formula

$$T_{si} = \frac{\frac{(T_i+T_{i+N})}{2} + T_{i+1} \cdots + T_{i+N-1}}{N} \tag{1}$$

where $T_{si}$ is the torque value with skewing at point $i$, $T_i$ is the torque value at point $i$ without skewing, and $N$ = skew angle/step length $\Delta\theta$ [7]. A linearization is involved to approximate the skewing effects using (1) based on 2-D FEA although the nonlinear effect due to the variations of flux in axial direction is usually negligible. If the origin of the torque waveform is placed at the center of the skewing, the above equivalent method of skewing will not introduce any phase shift, which can be briefly proved as follows.

It can be assumed that the fundamental component of the torque waveform computed by FEA as shown in Fig. 5 is approximately represented by

$$T_1(\theta) = T_{1\text{peak}} \sin\theta \tag{2}$$

where $\theta$ is the angle between the center axis of the rotor MMF and that of the stator MMF in electrical degrees. Since the origin of the waveform is at the center of the skewing, the integration (or averaging) region should be from $-\alpha/2$ to $\alpha/2$, where $\alpha$ is the skew angle. The torque after averaging the values over the skew angle becomes

$$\begin{aligned} T_{1s}(\theta) =& \frac{1}{\alpha}\int_{\theta-\alpha/2}^{\theta+\alpha/2} T_1(\delta)d\delta = \frac{1}{\alpha}\int_{\theta-\alpha/2}^{\theta+\alpha/2} T_{1\text{pk}}\sin\delta d\delta \\ =& \frac{\sin\frac{\alpha}{2}}{\frac{\alpha}{2}} T_{1\text{pk}}\sin\theta. \end{aligned} \tag{3}$$

Therefore, the torque waveforms with and without skewing are in phase.

## IV. Simulation Results and Analysis

### A. Validation of the Simulation Results

FEA has been performed based on the above topology for various excitation currents: 25, 35, 45, 55, 65, and 75 A. Experimental tests have also been conducted. Electromagnetic torque has been computed while the rotor rotated from the position where the center axis of the rotor magnet MMF is 60° (mech.) apart from that of the stator MMF under a fixed switching pattern, to the position where the two center axes are aligned. The step length is 0.5° (mech.). For each excitation, a torque waveform with 121 points, as a function of rotor position, has been obtained by FEA.

The algorithm (1) for the skewing effect process has been applied to the torque waveforms obtained by FEA under different excitation currents. The effectiveness of skew in reducing the cogging torque has been demonstrated by the simulation results under zero stator current excitation, where the computed torque pulsation by FEA is nothing but the cogging torque (Fig. 6).

The processed torque waveforms over 120° (one electrical revolution) have been plotted together with the corresponding

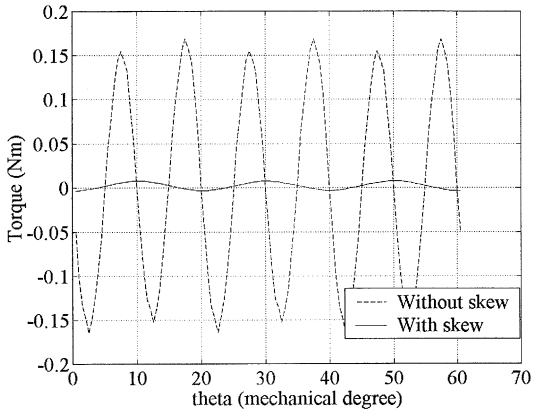


Fig. 6. Cogging torque with and without skewing.

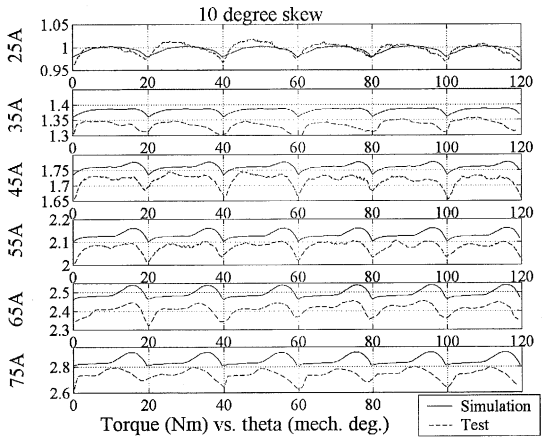


Fig. 7. Simulation and test torque waveforms under different currents over an electrical revolution (120° mech).

test results and shown in Fig. 7. The test results are obtained through torque measurement calibrated and kept under QS 9000 requirements. The accuracy is about $\pm 2.5$ mN-m. Fig. 7 shows that the simulation-based torque waveforms (10° skew) are generally close to the test results, except for two major differences. First, in most cases, the mean torque value of the simulation-based torque is slightly greater than that of the test-based torque. Second, the test torque exhibits a slightly more significant dip on top of each ripple. The first difference is due to the mechanical and core losses, measurement, modeling, and computation errors. The cause of the second difference will be explained later in this section.

Fourier contents of these signals have been computed to compare the simulation-based ripples with the test-based ones. The Fourier decomposition shows that the harmonics with an order above three are insignificant and negligible. Fig. 8 compares the magnitudes of the first three harmonics (the fundamental, the second, and third harmonics) of simulation data to the test-based ones under different excitations. Similarity between the two has been exhibited in that the absolute value differences between the two groups of data are in a reasonable range and the relative relation of the first three harmonics of the simulation data are generally the same as that of the test data. Please also note that the analysis did not consider miscellaneous effects like position sensor accuracy and skewing accuracy.

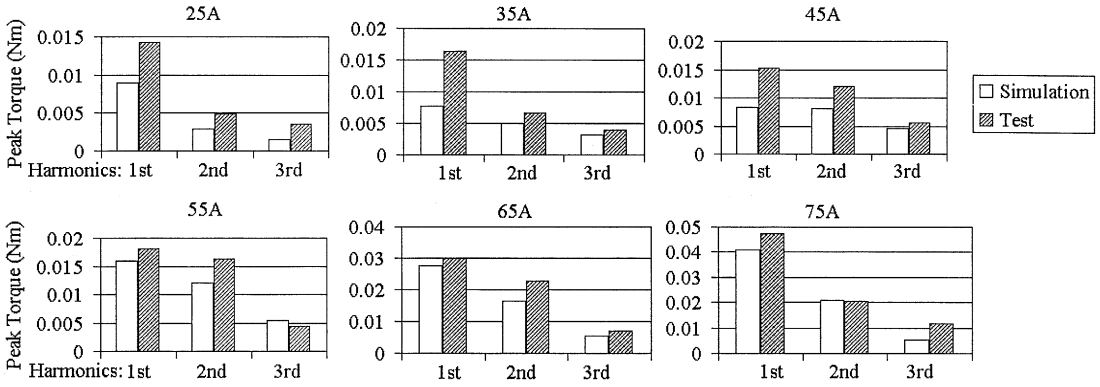


Fig. 8. Fourier contents in simulation and test torque ripples under different excitation currents.

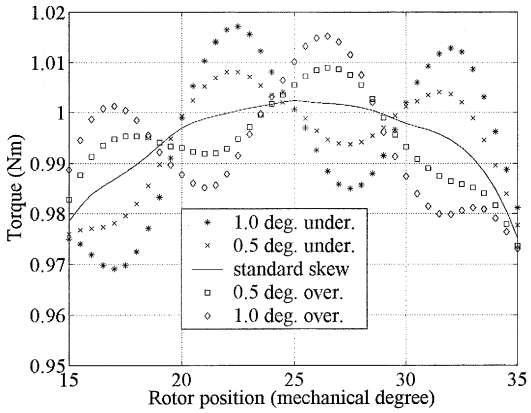


Fig. 9. Effects of underskew and overskew to the torque ripple at 25 A.

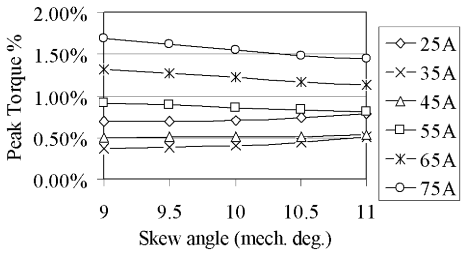


Fig. 10. Peak values of the fundamental torque ripple (six per electrical revolution) under different skew angles (in percentage of the corresponding dc component).

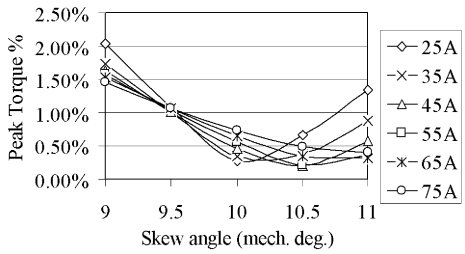


Fig. 11. Peak values of the second-order torque harmonics (12 per electrical revolution) under different skew angles (in percentage of the corresponding dc component).

In Fig. 8, the simulation results are provided with a skew of 10° (mech.). Because of the nonideal skewing and other effects, the tested machine had about 6 mN-m peak-to-peak cogging torque that is not included in the simulation. This torque ripple practically remains the same irrespective of the current. At small current, this becomes a large percentage of the total torque while at higher currents, this becomes an insignificant percentage of the total torque. This explains the cause of the difference between the simulation and test results in Fig. 8, and why it is smaller at higher current.

### *B. Effects of Underskew and Overskew*

In order to study the influence of various skewing angles on the torque waveforms, FEA and torque computation have also been performed for nonstandard skewing cases. Five skewing conditions have been studied—standard half stator slot skew (° skew, mech.), 0.5° underskew (9.5° skew), 1° underskew (9° skew), 0.5° overskew (10.5° skew), and 1° overskew (11° skew). Fig. 9 shows the torque waveforms under these skew conditions over a 20° (mech.) region for 25-A current excitation. The same simulations under other excitation currents have also been performed and the results are similar to the 25-A case.

From Fig. 9, it can be observed that generally either underskew or overskew increases the ripple on the torque waveform, and the greater the magnitude of underskew or overskew, the stronger the ripple. Underskew and overskew have opposite effects on the torque—for any rotor position, if underskew decreases the torque, then overskew must increases it, and vice versa. Moreover, each of the waveforms can be segmented into four sections approximately separated by the points at 20°, 25°, and 30° positions. The waveform within one section tends to have an increasing/decreasing trend opposite to that of the adjacent sections. Therefore, the shape of the torque waveforms, including the dips and the peaks, can be changed by skewing. Different skewing schemes, even though vary slightly, may reshape the torque waveform by changing a dip into a peak or vice versa. Based on the above discussion, underskew or overskew causes extra dips or peaks on the ripple. Therefore, it is very likely that the dips on the test based torque waveforms in Fig. 7 are caused by overskew or underskew due to manufacturing imperfection. This statement can be further confirmed by the successful repeat of the "moving" dip phenomenon using simulation under underskew condition shown in Section IV-C.

Underskew and overskew each have a different impact on different torque ripple harmonics. Figs. 10 and 11 illustrate the influences of skew angles on the fundamental torque ripple and the

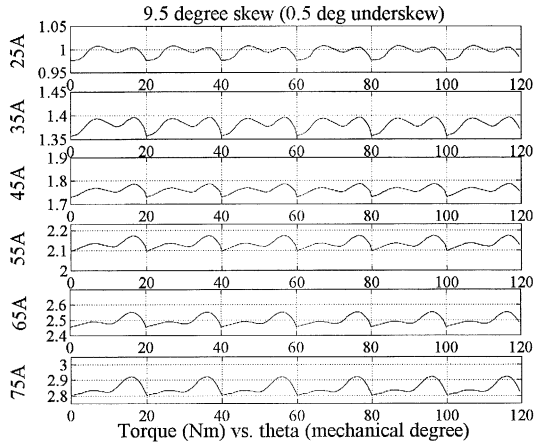


Fig. 12. "Moving" dip phenomenon shown by simulation.

second order torque ripple harmonics. The peak torque values of the fundamentals and the harmonics are represented as a percentage of the corresponding dc component of the ripple. According to Fig. 10, skew angle change does not affect the fundamental torque ripple significantly. However, based on Fig. 11, the skew angle greatly changes the magnitude of the second order torque ripple harmonics. For each individual excitation current, there exists an optimal skew angle where the magnitude of the second order harmonics is minimized. The optimal skew angle varies with excitation current—the greater the excitation current, the larger the optimal skew angle. The skew angle's impact on the second order torque ripple harmonics can also be seen from Fig. 9. Since the range of the figure covers one period in terms of the fundamental ripple, it is apparent that all of the ripples imposed on the 10° skew torque curve are the second order harmonics. Since the skew angle does not influence the fundamental torque ripple much, the overall torque ripple mainly depends on the second harmonics. It can be observed from Fig. 11 that a small overskew between 10 to 10.5° is ideal in minimizing the overall torque ripple, though it does increase the cogging torque, thus increasing the percentage torque ripple at lower current.

### C. "Moving" Dip

From Fig. 7, it can be observed that the position of the dip on the test-based torque waveform moves from the right side to the left side of a ripple when the excitation current increases from 25 to 75 A. This phenomenon can be reproduced by FEA simulation. Since a nonideal skew angle could produce a dip on a torque ripple, a 9.5° skew angle has been used in the simulation to reproduce the "moving" dip phenomenon. The simulation result is shown in Fig. 12. In Fig. 12, it is apparent that the dip makes two peaks (i.e., the left peak and the right peak), on one ripple. Fig. 13 shows the relations between the two peaks when current changes.

According to Fig. 13, the height of the left peak does not change when excitation current increases while the height of the right peak increases linearly when current increases. At low current, the right peak is lower than the left one and the dip appears to be at the right side of the ripple. However, at high current, the right peak is higher than the left one and accordingly

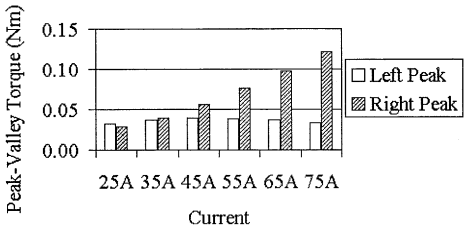


Fig. 13. Heights of the left and right peak on a torque ripple under different currents.

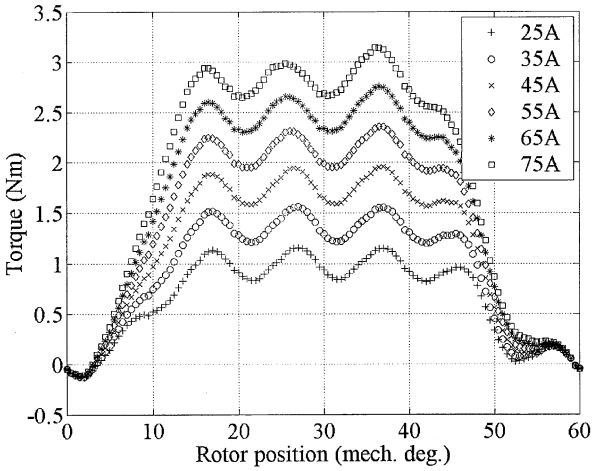


Fig. 14. Simulation torque over 60° (mech.) without skewing.

the dip seems to be at the left side of the ripple. Therefore, the cause of the "moving" dip is the height change of the right peak when current changes.

By definition, cogging torque is not related to stator current. However, due to the operating principle, under any switching pattern, only two of the three phases are conducting. Therefore, the tooth flux density will not be evenly distributed along the air-gap (i.e., flux density is stronger under some teeth and weaker under others due to the stator current), or affected more by stator current under some teeth and less under others. Consequently, this unevenness of tooth flux density causes additional current related "cogging" torque component. This current related "cogging" torque cannot be 100% eliminated by skewing. Fig. 14 demonstrates the existence of the current-related "cogging" (notice the peaks at about 37°).

The successful repeat of the "moving" dip phenomenon, which is observed from the test results, using simulation under underskew condition has additionally demonstrated that the cause of the observed dip is caused by the nonstandard skew.

## V. Conclusion

FEA-based simulations have been performed to compute the torque waveforms of a PM brushless dc motor under different excitations. The computed torque waveforms have been validated using the experimental data measured under the same conditions. For the motor analyzed in this paper, the following conclusions can be drawn on the basis of the above discussions:

Both underskew and overskew have significant impacts on the torque waveform. The dip on the test-based torque ripple

is caused by a nonideal skew angle due to manufacturing inaccuracy. The skew angle influences the torque ripple mainly by affecting its second-order harmonics. Under a certain current, an optimal skew angle exists in terms of the second-order torque ripple harmonics, where it is minimized. The optimal skew angle increases from the standard skew angle while excitation current increases. For the machine configuration analyzed in this paper, a small overskew between 10° and 10.5° is ideal in minimizing the overall torque ripple, though it is adding the cogging torque, thus increasing the percentage torque ripple at lower current. Also for this machine, there are two peaks on the torque waveform within the 20° (mech.) switching period. The change of the relative heights of the two peaks causes the "moving" dip.

## REFERENCES


[1] M. Lajoie-Mazenc, B. Nogarede, and J. C. Fagundes, "Analysis of torque ripple in electronically commutated permanent magnet machines and minimization methods," in *Proc. Inst. Elect. Eng. Conf. Publ.*, 1989, pp. 85–89.

[2] G. H. Jang and D. K. Lieu, "Vibration reduction in electric machine by magnet interlacing," *IEEE Trans. Magn.*, vol. 28, pp. 3024–3026, Sept. 1992.

[3] S. M. Hwang and D. K. Lieu, "Reduction of torque ripple in brushless DC motors," *IEEE Trans. Magn.*, pt. 2, vol. 31, pp. 3737–3739, Nov. 1995.

[4] J. S. Hsu, B. P. Scoggins, M. B. Scudiere, L. D. Marlino, D. J. Adams, and P. Pillay, "Nature and assessments of torque ripples of permanent-magnet adjustable-speed motors," in *Proc. IEEE Ind. Applicat. Soc. Annu. Meet.*, vol. 3, Orlando, FL, Oct. 1995, pp. 2696–2702.

[5] R. P. Deodhar, D. A. Staton, and T. J. E. Miller, "Modeling of skew using the flux-MMF diagram," *IEEE Trans. Ind. Applicat.*, vol. 32, pp. 1339–1347, Nov./Dec. 1996.

[6] T. Y. Chuang, D. K. Lieu, and J. S. McAllister, "Optimization of pole and slot widths for reluctance torque reduction in a brushless DC spindle motor," in *Proc. Amer. Soc. Mech. Eng., Inform. Storage Processing Division*, vol. 2, Atlanta, GA, Nov. 1996, pp. 153–158.

[7] M. Sunil, D. Benoit, B. Liu, and T. S. Sebastian, "Minimization of torque pulsations in a trapezoidal back-EMF permanent magnet brushless dc motor," in *Proc. IEEE Ind. Applicat. Soc. Annu. Meet.*, vol. 2, Phoenix, AZ, Oct. 1999, pp. 1237–1242.

[8] S. Salon, K. Sivasubramaniam, and L. Tukenmez-Ergene, "An approach for determining the source of torque harmonics in brushless dc motors," in *Proc. Int. Conf. Elect. Mach.*, vol. 3, Espoo, Finland, Aug. 2000, pp. 1707–1711.

[9] M. Lukaniszyn and R. Wrobel, "Study on the influence of permanent magnet dimensions and stator core structures on the torque of the disc-type brushless DC motor," *Elect. Eng.*, vol. 82, no. 3, pp. 163–171, 2000.

[10] S. C. Park, T. H. Yoon, B. I. Kwon, H. S. Yoon, and S. H. Won, "Influence on brushless DC motor performance due to unsymmetric magnetization distribution in permanent magnet," *IEEE Trans. Magn.*, vol. 36, pp. 1898–1901, July 2000.

[11] S. M. Hwang, J. B. Eom, G. B. Hwang, W. B. Jeong, and Y. H. Jung, "Cogging torque and acoustic noise reduction in permanent magnet motors by teeth pairing," *IEEE Trans. Magn.*, vol. 36, pp. 3144–3146, Sept. 2000.

[12] T. Ohnishi and N. Takahashi, "Optimal design of efficient IPM motor using finite element method," *IEEE Trans. Magn.*, vol. 36, pp. 3537–3539, Sept. 2000.

[13] C. Breton, J. Bartolome, J. A. Benito, G. Tassinario, I. Flotats, C. W. Lu, and B. J. Chalmers, "Influence of machine symmetry on reduction of cogging torque in permanent-magnet brushless motors," *IEEE Trans. Magn.*, vol. 36, pp. 3819–3823, Sept. 2000.

[14] Z. Q. Zhu and D. Howe, "Influence of design parameters on cogging torque in permanent magnet machines," *IEEE Trans. Energy Conversion*, vol. 15, pp. 407–412, Dec. 2000.

[15] F. Caricchi, F. Crescimbini, G. Capponi, and L. Solero, "Novel solid-state-commutator PM motor arrangement for EV application," in *Proc. IEEE Ind. Applicat. Soc. Annu. Meeting*, Phoenix, AZ, Oct. 1999, pp. 2545–2551.

[16] R. Krishnan and P. V. Vijayraghavan, "New power converter topology for PM brushless DC motor drives," in *Proc. Ind. Electron. Soc. Anuu. Conf.*, vol. 2, Aachen, Germany, Aug. 1998, pp. 709–714.

[17] B. S. Lee and R. Krishnan, "Variable voltage converter topology for permanent-magnet brushless DC motor drives using buck-boost front-end power stage," in *IEEE Int. Symp. Ind. Electron.*, vol. 2, Bled, Slovenia, July 1999, pp. 689–694.

[18] T. Sebastian and V. Gangla, "Analysis of induced EMF waveforms and torque ripple in a brushless permanent magnet machine," *IEEE Trans. Ind. Applicat.*, vol. 32, pp. 195–200, Jan./Feb. 1996.

[19] S. Waikar, T. Gopalarathnam, H. A. Toliyat, and J. C. Moreira, "Evaluation of multiphase brushless permanent magnet (BPM) motors using finite element method (FEM) and experiments," in *Proc. IEEE Appl. Power Electron. Conf. Exposition*, vol. 1, Dallas, TX, Mar. 1999, pp. 396–402.

[20] *FLUX2D Version 7.40 User's Guide*, Magsoft Corporation, 1999.

[21] S. J. Salon, *Finite Element Analysis of Electrical Machines*. Norwell, MA: Kluwer, 1995.



**Min Dai** (S'99) was born in Shanghai, China, in 1971. He received the B.S. and M.S. degrees in electrical engineering from Tsinghua University, Beijing, China, in 1994 and 1997, respectively, and the M.S. degree in computer science from the University of Alabama, Huntsville, in 1999. He is currently pursuing the Ph.D. degree at The Ohio State University, Columbus.

His current research at OSU includes electrical machines and variable speed drives, control in power electronic systems, and distributed power systems. From 1993 to 1997, he was with the State Key Lab of Intelligent Technology and Systems at Tsinghua University working on robotics and intelligent control. From 1997 to 1999, he was a Research Assistant in the Visualization Lab at the University of Alabama, working on computer vision and three-dimensional object recognition.

**Ali Keyhani** (F'98) is the Director of the Department of Electrical Engineering at Mechatronic Systems Laboratory at The Ohio State University (OSU), Columbus. He was a Consultant to Accuray, Columbus; Combustion Engineering, Columbus; TRW Controls, Houston, TX; Liebert, Delaware, OH; Delphi Automotive Systems; Mahab Engineering, Tehran, Iran; and Foster Wheeler Engineering, Tehran, Iran. His research interests include mechatronic/electromechanical systems, power systems, hybrid electric vehicles, power electronics, design of electric machines, finite element modeling, digital signal processing, parameter estimation, and control of electromechanical systems.

He has authored many IEEE Transactions papers on control of power systems, machine modeling, parameter estimation, power electronic systems, and design of virtual and test beds for variable speed drive systems.

Dr. Keyhani is the Chairman of the Electric Machinery Committee and the past editor of IEEE TRANSACTIONS ON ENERGY CONVERSION. He established the OSU Mechatronic graduate program in 1995. Dr. Keyhani is a recipient of The OSU College of Engineering Research Award for 1989 and 1999.

**Tomy Sebastian** (S'80–S'84–M'84–M'86–SM'94) received the B.Sc. (Eng.) degree from Regional Engineering College, Calicutta, India, in 1979, the M.S. degree from Indian Institute of Technology, Madras, India, in 1982, and the MA.Sc. and Ph.D. degrees from the University of Toronto, Toronto, ON, Canada, in 1984 and 1986, respectively.

Currently, he is with the Advanced Engineering Center of Delphi Saginaw Steering Systems, Delphi Automotive Systems, Saginaw, MI, where he leads the advanced motor development activities. He also holds an adjunct faculty position at The Ohio State University, Columbus. From 1979 to 1980, he was with the R&D Center of KELTRON, Trivandrum, India. From 1987 to 1992, he was with the Research and Applied Technology Division of Black and Decker Corporation, Towson, MD. His areas of interest are electrical machines and variable speed drives.

Dr. Sebastian is corecipient of an IEEE Industry Application Society Transactions First-Prize Paper Award. He is the Vice-Chairman for paper reviews for the Industrial Power Conversion Department of the IEEE Industry Applications Society.